Mechanics of Advanced Materials and Structures, 18:133–146, 2011

ISSN: 1537-6494 print / 1537-6532 online
DOI: 10.1080/15376494.2010.496067

Taylor & Francis
Taylor & Francis Group

Exact Geometry Piezoelectric Solid-Shell Element Based on the 7-Parameter Model

G. M. Kulikov and S. V. Plotnikova
Department of Applied Mathematics and Mechanics, Tambov State Technical University, Tambov, Russia

The present work focuses on the development of the exact geometry piezoelectric four-node solid-shell element based on the first-order 7-parameter equivalent single-layer theory, which permits to utilize the 3D constitutive equations. The term "exact geometry" reflects the fact that the reference surface geometry is described by analytically given functions, in particular spline functions, and displacement vectors are resolved in the reference surface frame. As fundamental shell unknowns, 6 displacements of the outer surfaces and a transverse displacement of the midsurface are chosen. Such choice of displacements gives the possibility to derive strain-displacement relationships, which are invariant under rigid-body shell motions in a convected curvilinear coordinate system. To avoid shear and membrane locking and have no spurious 0 energy modes, the assumed strain and stress resultant fields are invoked. It is noteworthy that the elemental matrices of the hybrid method developed require only direct substitutions, i.e., no expensive matrix inversion is needed and they are evaluated by using the 3D analytical integration.

Keywords piezoelectric laminated shell, exact geometry four-node solid-shell element, 7-parameter shell model

1. INTRODUCTION

Extensive work has been carried out on the 3D continuum-based finite elements that can handle analyses of thin piezoelectric laminated composite shells satisfactorily [1, 2]. These elements typically are defined by two layers of nodes at the bottom and top surfaces of the shell with three displacement degrees of freedom per node and known as isoparametric 6-parameter piezoelectric solid-shell elements. In the isoparametric solid-shell element formulation, initial and deformed geometry are equally interpolated allowing one to describe rigid-body motions precisely. The development of 6-parameter piezoelectric solid-shell elements was not straightforward. In order to overcome element deficiencies such as shear, membrane, and curvature thickness locking, the ANS hybrid stress [3], hybrid strain [4], hybrid stress-strain [5–7] and enhanced assumed strain (EAS) [5–8] finite element formulations were applied. Still, the isoparametric piezoelectric solid-shell element formulation is computationally inefficient because stresses and strains are analyzed in the global and local orthogonal Cartesian coordinate systems, although the normalized element coordinates represent already convected curvilinear coordinates.

One can arrive at a more efficient finite element formulation utilizing the exact geometry (EG) piezoelectric solid-shell elements that finds its point of departure in papers [9, 10]. The EG piezoelectric solid-shell element formulation is based on the strain-displacement relationships of the first-order 6-parameter equivalent single-layer (ESL) theory. It is worth noting that these strain-displacement relationships precisely represent all rigid-body shell motions in any convected curvilinear coordinate system and no assumptions except for Timoshenko-Mindlin kinematics are required to derive them [11, 12]. For this purpose, the displacement vectors of bottom and top surfaces of the shell are introduced but resolved, in contrast with the isoparametric solid-shell element formulation, in the reference surface frame.

It is well known that the 6-parameter piezoelectric solid-shell formulation on the basis of the complete 3D constitutive equations is deficient because thickness locking occurs. This is due to the fact that the linear displacement field in the thickness direction results in a constant transverse normal strain, which in turn causes artificial stiffening of the shell element in the case of non-vanishing Poisson's ratios. In order to circumvent a locking phenomenon, the 3D constitutive equations have to be modified [4, 9]. However, the use of complete 3D constitutive laws within the piezoelectric shell analysis is of great importance for engineering applications [13]. Thus, the first-order 7-parameter ESL piezoelectric shell model is best suited for this purpose because such a model is optimal with respect to the number of degrees of freedom employed [14, 15]. The proposed 7-parameter ESL piezoelectric shell model is based on introducing six displacements of the outer surfaces and a transverse displacement of the midsurface as fundamental shell unknowns. Such choice of displacements gives the possibility to represent the EG solid-shell element formulation in a very compact form and to derive strain-displacement relationships,

Address correspondence to Prof. G. M. Kulikov, Department of Applied Mathematics and Mechanics, Tambov State Technical University, Sovetskaya Street 106, Tambov 392000, Russia. E-mail: gmkulikov@mail.ru and kulikov@apmath.tstu.ru

which are invariant again under rigid-body motions in convected curvilinear coordinates [15].

It is assumed that the electric potential is linear through the thickness of the piezoelectric layer and all displacement and electric potential degrees of freedom are coupled via 3D constitutive equations. The first assumption means that the electric field is constant through the thickness of the piezoelectric layer, which is not correct in bending dominated situations (see, e.g. [16]). Note also that the electric charge conservation law never can be satisfied precisely. The analytical developments for piezoelectric beams [17] and plates [18] showed that the quadratic variation of the electric potential in the thickness direction is sufficient to solve this problem. However, the quadratic approximation of the electric potential leads to including additional degrees of freedom in a finite element formulation and seems to be excessive for the actuator shell analysis.

To avoid shear and membrane locking and have no spurious zero energy modes, the assumed strain and stress resultant fields are invoked. This approach was developed for the 6- and 7-parameter EG solid-shell element formulations in [9, 11, 15]. Herein, the above hybrid stress-strain formulation is extended to the EG piezoelectric four-node solid-shell element based on the first-order 7-parameter ESL shell theory. Taking into account that displacement vectors of outer and middle surfaces of the shell are resolved in the reference surface frame, the proposed EG piezoelectric solid-shell element formulation has computational advantages compared to the conventional isoparametric solid-shell element formulations, since it reduces the computational cost of numerical integration in the evaluation of the stiffness matrix. This is due to the fact that, first, the element matrix developed requires only direct substitutions, i.e., no numerical matrix inversion is needed. The latter is unusual for the isoparametric hybrid/mixed shell element formulations. Secondly, we use the efficient 3D analytical integration [19] that permits to employ coarse meshes.

2. STRAIN-DISPLACEMENT RELATIONSHIPS

Consider a shell built up in the general case by the arbitrary superposition across the wall thickness of N thin layers of the uniform thickness $h_n = z_n - z_{n-1}$ including the ℓth piezoelectric layer (PZT) as shown in Figure 1. The nth layer may be defined as a 3D body of volume V_n bounded by two surfaces Ω_{n-1} and Ω_n, located at the distances $|z_{n-1}|$ and $|z_n|$ measured with respect to the reference surface Ω, and the edge boundary surface Σ_n. It is assumed that the bounding surfaces Ω_{n-1} and Ω_n are continuous, sufficiently smooth and without any singularities. Let the reference surface Ω be referred to the orthogonal curvilinear coordinates θ_1 and θ_2, which are referred to the lines of principal curvatures of its surface, whereas the coordinate θ_3 is oriented along the unit vector $\mathbf{e}_3$ normal to the reference surface; $\mathbf{e}_1$ and $\mathbf{e}_2$ are the unit vectors tangent to the lines of principal curvatures. Here and in the following developments, the index n identifies the belonging of any quantity to the nth layer and runs from 1 to N; the index of the piezoelectric layer $\ell = i_1,\ i_2, \ldots, i_L$, where L is the number of piezoelectric layers bonded to the outer surfaces of the host structure or embedded into its body; Greek indices α, β range from 1 to 2; indices i, j range from 1 to 3; the superscript A identifies the belonging of any quantity to the bottom and top surfaces Ω^- and Ω^+, and takes values – and +.

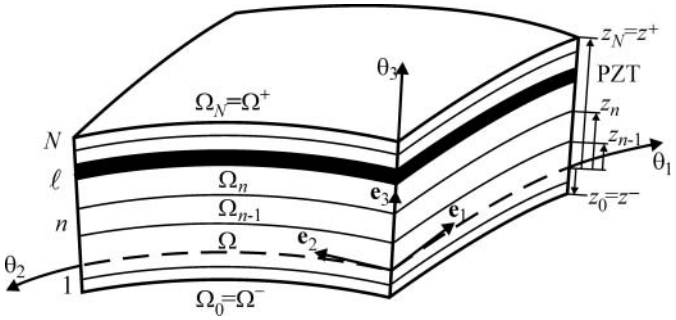

FIG. 1. Laminated shell with embedded piezoelectric layer (PZT).

The displacement field is approximated in the thickness direction according to [20]:

$$u_\alpha = N^- u_\alpha^- + N^+ u_\alpha^+, \quad u_3 = L^- u_3^- + L^M u_3^M + L^+ u_3^+, \tag{1}$$

$$N^- = \frac{1}{h}(z^+ - \theta_3), \qquad N^+ = \frac{1}{h}(\theta_3 - z^-), \tag{2}$$

$$L^- = N^-(N^- - N^+), \qquad L^M = 4N^- N^+, \qquad L^+ = N^+(N^+ - N^-), \tag{3}$$

where $N^A(\theta_3)$ and $L^A(\theta_3)$, $L^M(\theta_3)$ are the Lagrange polynomials of the first and second orders, respectively; $h = z^+ - z^-$ is the thickness of the shell; $z^- = z_0$ and $z^+ = z_N$ are the transverse coordinates of bottom and top surfaces of the shell; $u_i^A(\theta_1, \theta_2)$ are the components of the displacement vectors of the bottom and top surfaces; $u_3^M(\theta_1, \theta_2)$ is the transverse displacement of the midsurface Ω^M.

Next, we represent displacement vectors of outer surfaces in the reference surface frame as follows:

$$\mathbf{u}^A = \sum_i u_i^A \mathbf{e}_i. \tag{4}$$

Therefore, the strain-displacement relationships of the first-order[1] 7-parameter shell model [15] can be written as

$$\varepsilon_{\alpha\beta} = N^- \varepsilon_{\alpha\beta}^- + N^+ \varepsilon_{\alpha\beta}^+, \qquad \varepsilon_{33} = N^- \varepsilon_{33}^- + N^+ \varepsilon_{33}^+, \tag{5}$$

$$\varepsilon_{\alpha 3} = \varepsilon_{\alpha 3}^{\mathrm{M}}, \qquad \varepsilon_{\alpha 3}^{\mathrm{M}} = \frac{1}{2}\left(\varepsilon_{\alpha 3}^- + \varepsilon_{\alpha 3}^+\right).$$

[1]This is due to the linear strain distribution through the thickness of the shell (see Arciniega and Reddy [14])

Here, $\varepsilon_{ij}^{A}(\theta_1,\ \theta_2)$ are the components of the strain tensor of outer surfaces of the shell expressed as

$$2\varepsilon_{\alpha\beta}^{A} = c_{\alpha}^{A}\lambda_{\alpha\beta}^{A} + c_{\beta}^{A}\lambda_{\beta\alpha}^{A}, \qquad \varepsilon_{33}^{A} = \beta_{3}^{A}, \tag{6}$$
$$2\varepsilon_{\alpha 3}^{A} = c_{\alpha}^{A}\beta_{\alpha}^{A} + \lambda_{3\alpha}^{A},$$

where

$$\lambda_{\alpha\alpha}^{A} = \frac{1}{A_\alpha}u_{\alpha,\alpha}^{A} + B_\beta u_\beta^A + k_\alpha u_3^A \quad \text{for } \beta \neq \alpha, \tag{7}$$
$$\lambda_{\beta\alpha}^{A} = \frac{1}{A_\alpha}u_{\beta,\alpha}^{A} - B_\beta u_\alpha^A \quad \text{for } \beta \neq \alpha,$$
$$\lambda_{3\alpha}^{A} = \frac{1}{A_\alpha}u_{3,\alpha}^{A} - k_\alpha u_\alpha^A, \qquad \beta_\alpha^A = \frac{1}{h}\left(u_\alpha^+ - u_\alpha^-\right),$$
$$\beta_3^- = \frac{1}{h}\left(-3u_3^- + 4u_3^M - u_3^+\right), \quad \beta_3^+ = \frac{1}{h}\left(u_3^- - 4u_3^M + 3u_3^+\right),$$
$$c_\alpha^A = 1 + k_\alpha z^A, \qquad B_\alpha = \frac{1}{A_\alpha A_\beta}A_{\beta,\alpha} \quad \text{for } \beta \neq \alpha,$$

where A_α and k_α are the Lamé coefficients and principal curvatures of the reference surface; c_α^A are the components of the shifter tensor at outer surfaces of the shell; the abbreviation $(\ )_{,\alpha}$ implies the partial derivatives with respect to coordinates θ_α. It is noteworthy that strain-displacement relationships (5) and (6) exactly represent all rigid-body shell motions in any convected curvilinear coordinate system [15].

3. DESCRIPTION OF ELECTRIC FIELD

The electric potential inside the ℓth piezoelectric layer is also assumed to be linear in the thickness direction

$$\varphi_\ell = N_\ell^- \varphi_\ell^- + N_\ell^+ \varphi_\ell^+, \tag{8}$$
$$N_\ell^- = \frac{1}{h_\ell}(z_\ell - \theta_3), \qquad N_\ell^+ = \frac{1}{h_\ell}(\theta_3 - z_{\ell-1}), \tag{9}$$

where $\varphi_\ell^A(\theta_1,\ \theta_2)$ are the values of the electric potential on the bottom and top surfaces of the ℓth layer; $h_\ell = z_\ell - z_{\ell-1}$ is the thickness of the piezoelectric layer.

The relation between the electric field $\mathbf{E}^{(\ell)}$ and the electric potential φ_ℓ is given by

$$\mathbf{E}^{(\ell)} = -\nabla\varphi_\ell, \tag{10}$$

that is,

$$E_\alpha^{(\ell)} = N_\ell^- E_\alpha^{(\ell)-} + N_\ell^+ E_\alpha^{(\ell)+}, \quad E_3^{(\ell)} = -\frac{1}{h_\ell}\left(\varphi_\ell^+ - \varphi_\ell^-\right), \tag{11}$$
$$E_\alpha^{(\ell)-} = -\frac{1}{A_\alpha}\varphi_{\ell,\alpha}^-, \qquad E_\alpha^{(\ell)+} = -\frac{1}{A_\alpha}\varphi_{\ell,\alpha}^+,$$

where $E_\alpha^{(\ell)A}$ are the tangential components of the electric field of the ℓth layer. It is seen that the normal component of the electric field $E_3^{(\ell)}$ is constant through the thickness of the piezoelectric layer. A short discussion of that is presented in the Introduction.

4. CONSTITUTIVE EQUATIONS

The constitutive equations of linear piezoelectricity for the monoclinic piezoelectric layer with reflectional symmetry in surfaces parallel to the reference surface can be expressed as

$$\bar{\varepsilon} = \mathbf{A}^{(\ell)}\boldsymbol{\sigma}^{(\ell)} + \left(\mathbf{d}^{(\ell)}\right)^T \mathbf{E}^{(\ell)}, \tag{12}$$
$$\mathbf{D}^{(\ell)} = \mathbf{d}^{(\ell)}\boldsymbol{\sigma}^{(\ell)} + \boldsymbol{\varsigma}^{(\ell)}\mathbf{E}^{(\ell)}, \tag{13}$$

where $\bar{\varepsilon}$ is the strain vector; $\boldsymbol{\sigma}^{(\ell)}$ is the stress vector; $\mathbf{E}^{(\ell)}$ is the electric field vector; $\mathbf{D}^{(\ell)}$ is the electric displacement vector; $\mathbf{A}^{(\ell)}$ is the elastic compliance matrix; $\mathbf{d}^{(\ell)}$ is the piezoelectric matrix; $\boldsymbol{\varsigma}^{(\ell)}$ is the dielectric matrix defined by

$$\bar{\varepsilon} = [\varepsilon_{11}\ \varepsilon_{22}\ \varepsilon_{33}\ 2\varepsilon_{23}\ 2\varepsilon_{13}\ 2\varepsilon_{12}]^{\mathrm{T}},$$
$$\boldsymbol{\sigma}^{(\ell)} = [\sigma_{11}^{(\ell)}\ \sigma_{22}^{(\ell)}\ \sigma_{33}^{(\ell)}\ \sigma_{23}^{(\ell)}\ \sigma_{13}^{(\ell)}\ \sigma_{12}^{(\ell)}]^{\mathrm{T}}, \tag{14}$$
$$\mathbf{E}^{(\ell)} = [E_1^{(\ell)}\ E_2^{(\ell)}\ E_3^{(\ell)}]^{\mathrm{T}}, \qquad \mathbf{D}^{(\ell)} = [D_1^{(\ell)}\ D_2^{(\ell)}\ D_3^{(\ell)}]^{\mathrm{T}},$$

$$\mathbf{A}^{(\ell)} = \begin{bmatrix} A_{11}^{(\ell)} & A_{12}^{(\ell)} & A_{13}^{(\ell)} & 0 & 0 & A_{16}^{(\ell)} \\ & A_{22}^{(\ell)} & A_{23}^{(\ell)} & 0 & 0 & A_{26}^{(\ell)} \\ & & A_{33}^{(\ell)} & 0 & 0 & A_{36}^{(\ell)} \\ & & & A_{44}^{(\ell)} & A_{45}^{(\ell)} & 0 \\ & & & & A_{55}^{(\ell)} & 0 \\ \text{sym.} & & & & & A_{66}^{(\ell)} \end{bmatrix}, \tag{15}$$

$$\mathbf{d}^{(\ell)} = \begin{bmatrix} 0 & 0 & 0 & d_{14}^{(\ell)} & d_{15}^{(\ell)} & 0 \\ 0 & 0 & 0 & d_{24}^{(\ell)} & d_{25}^{(\ell)} & 0 \\ d_{31}^{(\ell)} & d_{32}^{(\ell)} & d_{33}^{(\ell)} & 0 & 0 & d_{36}^{(\ell)} \end{bmatrix},$$

$$\boldsymbol{\varsigma}^{(\ell)} = \begin{bmatrix} \varsigma_{11}^{(\ell)} & \varsigma_{12}^{(\ell)} & 0 \\ & \varsigma_{22}^{(\ell)} & 0 \\ \text{sym.} & & \varsigma_{33}^{(\ell)} \end{bmatrix}.$$

Solving constitutive Eqs. (12) for stresses and substituting stresses in constitutive Eqs. (13), one obtains

$$\boldsymbol{\sigma}^{(\ell)} = \mathbf{C}^{(\ell)}\bar{\varepsilon} - \left(\mathbf{e}^{(\ell)}\right)^{\mathrm{T}}\mathbf{E}^{(\ell)}, \tag{16}$$
$$\mathbf{D}^{(\ell)} = \mathbf{e}^{(\ell)}\bar{\varepsilon} + \in^{(\ell)}\mathbf{E}^{(\ell)}, \tag{17}$$

where $\mathbf{C}^{(\ell)}$ is the material stiffness matrix; $\mathbf{e}^{(\ell)}$ and $\in^{(\ell)}$ are the piezoelectric and dielectric matrices expressed as

$$\mathbf{C}^{(\ell)} = \left(\mathbf{A}^{(\ell)}\right)^{-1},\ \mathbf{e}^{(\ell)} = \mathbf{d}^{(\ell)}\mathbf{C}^{(\ell)},$$
$$\in^{(\ell)} = \boldsymbol{\varsigma}^{(\ell)} - \mathbf{d}^{(\ell)}\mathbf{C}^{(\ell)}(\mathbf{d}^{(\ell)})^{\mathrm{T}}. \tag{18}$$

5. HU-WASHIZU VARIATIONAL EQUATION

The first-order 7-parameter piezoelectric ESL shell theory developed is based on the approximations of displacements (1), displacement-dependent strains (5), electric potential (8) and electric field (11) in the thickness direction. Additionally, we accept the through-thickness approximation for the independently assumed strains as follows:

$$\hat{\varepsilon}_{\alpha\beta} = N^{-}\hat{\varepsilon}^{-}_{\alpha\beta} + N^{+}\hat{\varepsilon}^{+}_{\alpha\beta},\quad \hat{\varepsilon}_{33} = N^{-}\hat{\varepsilon}^{-}_{33} + N^{+}\hat{\varepsilon}^{+}_{33},\quad \hat{\varepsilon}_{\alpha3} = \hat{\varepsilon}^{\mathrm{M}}_{\alpha3}, \tag{19}$$

where $\hat{\varepsilon}^{A}_{\alpha\beta}(\theta_1, \theta_2)$ and $\hat{\varepsilon}^{A}_{33}(\theta_1, \theta_2)$ are the assumed tangential and transverse normal strains of outer surfaces; $\hat{\varepsilon}^{M}_{\alpha3}(\theta_1, \theta_2)$ are the assumed transverse shear strains of the midsurface.

Substituting approximations (1), (5), (8), (11) and (19) into the 3D Hu-Washizu functional [9] and allowing for that metrics of all surfaces parallel to the reference surface are identical and equal to the metric of the midsurface, one arrives at the 2D Hu-Washizu functional for the 7-parameter shell element

$$\begin{aligned}\Pi^{\mathrm{el}}_{\mathrm{HW}} = \int_{-1}^{1}\int_{-1}^{1}\Big[&\frac{1}{2}\hat{\boldsymbol{\varepsilon}}^{\mathrm{T}}\mathbf{D}_{uu}\hat{\boldsymbol{\varepsilon}} - \hat{\boldsymbol{\varepsilon}}^{\mathrm{T}}\mathbf{D}^{(\ell)}_{u\varphi}\boldsymbol{E}^{(\ell)}\\ &-\frac{1}{2}\left(\boldsymbol{E}^{(\ell)}\right)^{\mathrm{T}}\mathbf{D}^{(\ell)}_{\varphi\varphi}\boldsymbol{E}^{(\ell)} - \mathbf{H}^{\mathrm{T}}(\hat{\boldsymbol{\varepsilon}} - \boldsymbol{\varepsilon})\\ &-\mathbf{v}^{\mathrm{T}}\mathbf{p} - \boldsymbol{\chi}^{\mathrm{T}}_{\ell}\mathbf{q}_{\ell}\Big]A_1A_2c^{\mathrm{M}}_1c^{\mathrm{M}}_2\ell_1\ell_2\mathrm{d}\xi_1\mathrm{d}\xi_2.\end{aligned} \tag{20}$$

Here, more convenient matrix notations are introduced

$$\begin{aligned}&\mathbf{v} = \left[u^{-}_1\ u^{-}_2\ u^{-}_3\ u^{+}_1\ u^{+}_2\ u^{+}_3\ u^{\mathrm{M}}_3\right]^{\mathrm{T}},\ \boldsymbol{\chi}_{\ell} = \left[\varphi^{-}_{\ell}\ \varphi^{+}_{\ell}\right]^{\mathrm{T}},\\ &\boldsymbol{\varepsilon} = \left[\varepsilon^{-}_{11}\ \varepsilon^{+}_{11}\ \varepsilon^{-}_{22}\ \varepsilon^{+}_{22}\ \varepsilon^{-}_{33}\ \varepsilon^{+}_{33}\ 2\varepsilon^{-}_{12}\ 2\varepsilon^{+}_{12}\ 2\varepsilon^{M}_{13}\ 2\varepsilon^{M}_{23}\right]^{\mathrm{T}},\\ &\hat{\boldsymbol{\varepsilon}} = \left[\hat{\varepsilon}^{-}_{11}\ \hat{\varepsilon}^{+}_{11}\ \hat{\varepsilon}^{-}_{22}\ \hat{\varepsilon}^{+}_{22}\ \hat{\varepsilon}^{-}_{33}\ \hat{\varepsilon}^{+}_{33}\ 2\hat{\varepsilon}^{-}_{12}\ 2\hat{\varepsilon}^{+}_{12}\ 2\hat{\varepsilon}^{M}_{13}\ 2\hat{\varepsilon}^{M}_{23}\right]^{\mathrm{T}},\\ &\mathbf{H} = \left[H^{-}_{11}\ H^{+}_{11}\ H^{-}_{22}\ H^{+}_{22}\ H^{-}_{33}\ H^{+}_{33}\ H^{-}_{12}\ H^{+}_{12}\ H_{13}\ H_{23}\right]^{\mathrm{T}},\\ &\boldsymbol{E}^{(\ell)} = \left[E^{(\ell)-}_1\ E^{(\ell)+}_1\ E^{(\ell)-}_2\ E^{(\ell)+}_2\ E^{(\ell)}_3\right]^{\mathrm{T}},\\ &\mathbf{p} = \left[-p^{-}_1\ -p^{-}_2\ -p^{-}_3\ p^{+}_1\ p^{+}_2\ p^{+}_3\ 0\right]^{\mathrm{T}},\quad \mathbf{q}_{\ell} = \left[q^{-}_{\ell}\ q^{+}_{\ell}\right]^{\mathrm{T}},\end{aligned} \tag{21}$$

where $\mathbf{D}_{uu}$, $\mathbf{D}^{(\ell)}_{u\varphi}$ and $\mathbf{D}^{(\ell)}_{\varphi\varphi}$ are the mechanical, piezoelectric and dielectric constitutive matrices presented in Appendix A; $\xi_{\alpha} = (\theta_{\alpha} - d_{\alpha})/\ell_{\alpha}$ are the normalized curvilinear elemental coordinates shown in Figure 2; d_{α} are the coordinates of the center of the element; $2\ell_{\alpha}$ are the lengths of the element in θ_{α}-directions; $c^{\mathrm{M}}_{\alpha} = 1 + k_{\alpha}z^{\mathrm{M}}$ are the components of the shifter tensor at the midsurface; $z^{\mathrm{M}} = (z^{-} + z^{+})/2$ is the transverse coordinate of the midsurface; p^{A}_{i} are the tractions applied to the bottom and top surfaces; q^{A}_{ℓ} are the prescribed surface charge densities of the ℓth piezoelectric layer; $H^{\pm}_{\alpha\beta}$, $H^{\pm}_{33}$ and $H_{\alpha3}$ are the stress resultants defined as

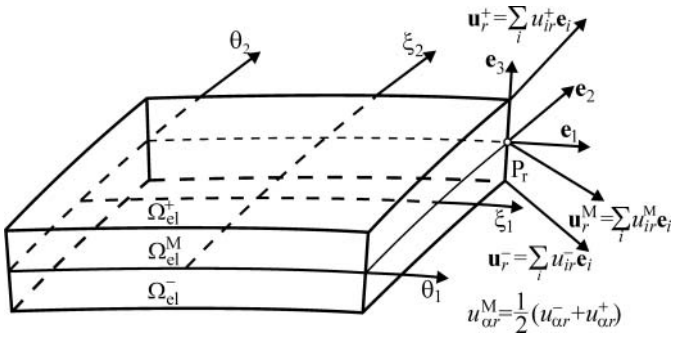

FIG. 2. EG piezoelectric solid-shell element based on the 7-parameter ESL shell model, where P_r is the element node ($r = 1, 2, \ldots, NN$).

$$\begin{aligned}&H^{A}_{\alpha\beta} = \sum_n\int_{z_{n-1}}^{z_n}\sigma^{(n)}_{\alpha\beta}N^{A}\mathrm{d}\theta_3,\qquad H^{A}_{33} = \sum_n\int_{z_{n-1}}^{z_n}\sigma^{(n)}_{33}N^{A}\mathrm{d}\theta_3,\\ &H_{\alpha3} = \sum_n\int_{z_{n-1}}^{z_n}\sigma^{(n)}_{\alpha3}\mathrm{d}\theta_3.\end{aligned} \tag{22}$$

Remark 1. For simplicity, we limit our discussion to the case of one piezoelectric layer, i.e., $L = 1$ and $\ell = i_1 \in \{1, 2, \ldots, N\}$, since only a sign of the summation needs to be involved in Eq. (20) to generalize.

Using the stationarity of the Hu-Washizu functional (20) with respect to independent variables $\mathbf{v}$, $\hat{\boldsymbol{\varepsilon}}$, $\mathbf{H}$ and $\boldsymbol{\chi}_{\ell}$, one can write the mixed variational equation as follows:

$$\delta\Pi^{\mathrm{el}}_{\mathrm{HW}} = 0. \tag{23}$$

6. FINITE ELEMENT FORMULATION

The finite element formulation is based on the simple and efficient approximation of shells via *curved four-node* piezoelectric solid-shell elements

$$\mathbf{v} = \sum_r N_r\mathbf{v}_r,\qquad \mathbf{v}_r = \left[u^{-}_{1r}\ u^{-}_{2r}\ u^{-}_{3r}\ u^{+}_{1r}\ u^{+}_{2r}\ u^{+}_{3r}\ u^{\mathrm{M}}_{3r}\right]^{\mathrm{T}}, \tag{24}$$

$$\boldsymbol{\chi}_{\ell} = \sum_r N_r\boldsymbol{\chi}_{\ell r},\qquad \boldsymbol{\chi}_{\ell r} = \left[\varphi^{-}_{\ell r}\ \varphi^{+}_{\ell r}\right]^{\mathrm{T}}, \tag{25}$$

$$N_r = \frac{1}{4}(1 + n_{1r}\xi_1)(1 + n_{2r}\xi_2), \tag{26}$$

$$n_{1r} = \begin{cases} 1 & \text{for } r = 1, 4\\ -1 & \text{for } r = 2, 3\end{cases},\qquad n_{2r} = \begin{cases} 1 & \text{for } r = 1, 2\\ -1 & \text{for } r = 3, 4\end{cases},$$

where $N_r(\xi_1,\ \xi_2)$ are the bilinear shape functions of the element; $\mathbf{v}_r$ and $\chi_{\ell r}$ are the displacement and electric potential vectors[2] of the element nodes; the index r runs from 1 to 4 and denotes the number of nodes

To implement the analytical integration throughout the element, we employ the *assumed interpolations* of natural strains and electric field vector as follows:

$$\boldsymbol{\varepsilon} = \sum_r N_r \boldsymbol{\varepsilon}_r, \qquad \boldsymbol{\varepsilon}_r = \boldsymbol{\varepsilon}\left(\mathrm{P}_r\right), \tag{27}$$

$$\boldsymbol{E}^{(\ell)} = \sum_r N_r E_r^{(\ell)}, \qquad \boldsymbol{E}_r^{(\ell)} = \boldsymbol{E}^{(\ell)}\left(\mathrm{P}_r\right). \tag{28}$$

The nodal values of strains of outer and middle surfaces according to Eqs. (5) and (6) are written as

$$\begin{aligned} 2\varepsilon^A_{\alpha\beta\, r} &= c^A_{\alpha\, r}\lambda^A_{\alpha\beta\, r} + c^A_{\beta\, r}\lambda^A_{\beta\alpha\, r}, \qquad \varepsilon^A_{33r} = \beta^A_{3r}, \\ 2\varepsilon^A_{\alpha 3r} &= c^A_{\alpha r}\beta^A_{\alpha r} + \lambda^A_{3\alpha r}, \qquad 2\varepsilon^{\mathrm{M}}_{\alpha 3r} = \varepsilon^-_{\alpha 3r} + \varepsilon^+_{\alpha 3r}, \end{aligned} \tag{29}$$

where $c^A_{\alpha r} = 1 + k_{\alpha r} z^A$ are the nodal values of the shifter tensor at outer surfaces. Introducing a displacement vector of the shell element

$$\mathbf{U} = \left[\mathbf{v}_1^{\mathrm{T}}\, \mathbf{v}_2^{\mathrm{T}}\, \mathbf{v}_3^{\mathrm{T}}\, \mathbf{v}_4^{\mathrm{T}}\right]^{\mathrm{T}}, \tag{30}$$

one derives the following key point presentation for the strain parameters:

$$\boldsymbol{\lambda}^A_{i\,\alpha r} = \left(\boldsymbol{\lambda}^A_{i\,\alpha r}\right)^{\mathrm{T}}\mathbf{U}, \qquad \beta^A_{ir} = \left(\boldsymbol{\Pi}^A_{ir}\right)^{\mathrm{T}}\mathbf{U}, \tag{31}$$

where $\boldsymbol{\lambda}^A_{i\,\alpha r}$ and $\boldsymbol{\Pi}^A_{ir}$ are the *constant* inside the element column matrices of order 28×1 given in Appendix B.

The use of Eqs. (27), (29) and (31) yields

$$\boldsymbol{\varepsilon}_r = \mathbf{B}^u_r \mathbf{U}, \tag{32}$$

where $\mathbf{B}^u_r$ are the strain-displacement transformation matrices of order 10×28 defined as

$$\mathbf{B}^u_r = \begin{bmatrix} c^-_{1r}\left(\boldsymbol{\Lambda}^-_{11r}\right)^{\mathrm{T}} \\ c^+_{1r}\left(\boldsymbol{\Lambda}^+_{11r}\right)^{\mathrm{T}} \\ c^-_{2r}\left(\boldsymbol{\Lambda}^-_{22r}\right)^{\mathrm{T}} \\ c^+_{2r}\left(\boldsymbol{\Lambda}^+_{22r}\right)^{\mathrm{T}} \\ \left(\boldsymbol{\Pi}^-_{3r}\right)^{\mathrm{T}} \\ \left(\boldsymbol{\Pi}^+_{3r}\right)^{\mathrm{T}} \\ \left(c^-_{1r}\boldsymbol{\Lambda}^-_{12r} + c^-_{2r}\boldsymbol{\Lambda}^-_{21r}\right)^{\mathrm{T}} \\ \left(c^+_{1r}\boldsymbol{\Lambda}^+_{12r} + c^+_{2r}\boldsymbol{\Lambda}^+_{21r}\right)^{\mathrm{T}} \\ \frac{1}{2}\left(c^-_{1r}\boldsymbol{\Pi}^-_{1r} + c^+_{1r}\boldsymbol{\Pi}^+_{1r} + \boldsymbol{\Lambda}^-_{31r} + \boldsymbol{\Lambda}^+_{31r}\right)^{\mathrm{T}} \\ \frac{1}{2}\left(c^-_{2r}\boldsymbol{\Pi}^-_{2r} + c^+_{2r}\boldsymbol{\Pi}^+_{2r} + \boldsymbol{\Lambda}^-_{32r} + \boldsymbol{\Lambda}^+_{32r}\right)^{\mathrm{T}} \end{bmatrix}. \tag{33}$$

Following a finite element technique developed and introducing the electric potential vector of the shell element

$$\boldsymbol{\Phi}_\ell = \left[\chi^{\mathrm{T}}_{\ell 1}\ \chi^{\mathrm{T}}_{\ell 2}\ \chi^{\mathrm{T}}_{\ell 3}\ \chi^{\mathrm{T}}_{\ell 4}\right]^{\mathrm{T}}, \tag{34}$$

we arrive at required relations

$$\boldsymbol{E}_r^{(\ell)} = -\mathbf{B}_r^{\varphi(\ell)}\boldsymbol{\Phi}_\ell. \tag{35}$$

Here, $\mathbf{B}_r^{\varphi(\ell)}$ are the piezoelectric transformation matrices of order 5×8 given by

$$\mathbf{B}_r^{\varphi(\ell)} = \left[\boldsymbol{\Xi}^-_{1r}\ \boldsymbol{\Xi}^+_{1r}\ \boldsymbol{\Xi}^-_{2r}\ \boldsymbol{\Xi}^+_{2r}\ \boldsymbol{\Xi}^{(\ell)}_{3r}\right]^{\mathrm{T}}, \tag{36}$$

where $\boldsymbol{\Xi}^A_{\alpha r}$ and $\boldsymbol{\Xi}^{(\ell)}_{3r}$ are the *constant* inside the element column matrices of order 8×1 presented in Appendix B.

From the computational point of view it is convenient to rewrite interpolations (27) and (28) as follows:

$$\boldsymbol{\varepsilon} = \sum_{r_1,\, r_2} (\xi_1)^{r_1}\,(\xi_2)^{r_2}\,\boldsymbol{\varepsilon}^{r_1 r_2}, \qquad \boldsymbol{\varepsilon}^{r_1 r_2} = \mathbf{B}_u^{r_1 r_2}\mathbf{U}, \tag{37}$$

$$\boldsymbol{E}^{(\ell)} = \sum_{r_1, r_2} (\xi_1)^{r_1}\,(\xi_2)^{r_2}\,\boldsymbol{E}^{(\ell) r_1 r_2}, \quad \boldsymbol{E}^{(\ell) r_1 r_2} = -\mathbf{B}_\varphi^{(\ell) r_1 r_2}\boldsymbol{\Phi}_\ell, \tag{38}$$

where the superscripts r_1, r_2 take the values 0 and 1, and

$$\begin{aligned} \mathbf{B}_u^{00} &= \frac{1}{4}\left(\mathbf{B}_1^u + \mathbf{B}_2^u + \mathbf{B}_3^u + \mathbf{B}_4^u\right), \\ \mathbf{B}_u^{01} &= \frac{1}{4}\left(\mathbf{B}_1^u + \mathbf{B}_2^u - \mathbf{B}_3^u - \mathbf{B}_4^u\right), \\ \mathbf{B}_u^{10} &= \frac{1}{4}\left(\mathbf{B}_1^u - \mathbf{B}_2^u - \mathbf{B}_3^u + \mathbf{B}_4^u\right), \\ \mathbf{B}_u^{11} &= \frac{1}{4}\left(\mathbf{B}_1^u - \mathbf{B}_2^u + \mathbf{B}_3^u - \mathbf{B}_4^u\right). \end{aligned} \tag{39}$$

[2]From this point, any vector of order M means the standard column matrix of order $\mathrm{M} \times 1$.

The matrices $\mathbf{B}_{\varphi}^{(\ell)r_1r_2}$ are obtained using matrices $\mathbf{B}_r^{\varphi(\ell)}$ in a similar manner.

To avoid shear and membrane locking and have no spurious zero energy modes, the assumed displacement-independent strain and stress resultant fields throughout the element [15] are invoked

$$\hat{\boldsymbol{\varepsilon}} = \sum_{r_1,\,r_2} (\xi_1)^{r_1}\,(\xi_2)^{r_2}\,\mathbf{Q}^{r_1\,r_2}\,\hat{\boldsymbol{\varepsilon}}^{r_1\,r_2}, \tag{40}$$

$$\hat{\boldsymbol{\varepsilon}}^{00} = \left[\hat{\varepsilon}_{11}^{-00}\ \hat{\varepsilon}_{11}^{+00}\ \hat{\varepsilon}_{22}^{-00}\ \hat{\varepsilon}_{22}^{+00}\ \hat{\varepsilon}_{33}^{-00}\ \hat{\varepsilon}_{33}^{+00}\ 2\hat{\varepsilon}_{12}^{-00}\ 2\hat{\varepsilon}_{12}^{+00}\ 2\hat{\varepsilon}_{13}^{\mathrm{M}00}\ 2\hat{\varepsilon}_{23}^{\mathrm{M}00}\right]^{\mathrm{T}},$$

$$\hat{\boldsymbol{\varepsilon}}^{01} = \left[\hat{\varepsilon}_{11}^{-01}\ \hat{\varepsilon}_{11}^{+01}\ \hat{\varepsilon}_{33}^{-01}\ \hat{\varepsilon}_{33}^{+01}\ 2\hat{\varepsilon}_{13}^{\mathrm{M}01}\right]^{\mathrm{T}},$$

$$\hat{\boldsymbol{\varepsilon}}^{10} = \left[\hat{\varepsilon}_{22}^{-10}\ \hat{\varepsilon}_{22}^{+10}\ \hat{\varepsilon}_{33}^{-10}\ \hat{\varepsilon}_{33}^{+10}\ 2\hat{\varepsilon}_{23}^{\mathrm{M}10}\right]^{\mathrm{T}},\quad \hat{\boldsymbol{\varepsilon}}^{11} = \left[\hat{\varepsilon}_{33}^{-11}\ \hat{\varepsilon}_{33}^{+11}\right]^{\mathrm{T}},$$

$$\mathbf{H} = \sum_{r_1,\,r_2} (\xi_1)^{r_1}\,(\xi_2)^{r_2}\,\mathbf{Q}^{r_1\,r_2}\mathbf{H}^{r_1\,r_2}, \tag{41}$$

$$\mathbf{H}^{00} = \left[H_{11}^{-00}\ H_{11}^{+00}\ H_{22}^{-00}\ H_{22}^{+00}\ H_{33}^{-00}\ H_{33}^{+00}\ H_{12}^{-00}\ H_{12}^{+00}\ H_{13}^{00}\ H_{23}^{00}\right]^{\mathrm{T}},$$

$$\mathbf{H}^{01} = \left[H_{11}^{-01}H_{11}^{+01}H_{33}^{-01}H_{33}^{+01}H_{13}^{01}\right]^{\mathrm{T}},$$

$$\mathbf{H}^{10} = \left[H_{22}^{-10}H_{22}^{+10}H_{33}^{-10}H_{33}^{+10}H_{23}^{10}\right]^{\mathrm{T}},\quad \mathbf{H}^{11} = \left[H_{33}^{-11}\ H_{33}^{+11}\right]^{\mathrm{T}},$$

where $\mathbf{Q}^{00}$ is the identity matrix of order 10×10, whereas

$$\mathbf{Q}^{01} = \begin{bmatrix} 1&0&0&0&0\\ 0&1&0&0&0\\ 0&0&0&0&0\\ 0&0&0&0&0\\ 0&0&1&0&0\\ 0&0&0&1&0\\ 0&0&0&0&0\\ 0&0&0&0&0\\ 0&0&0&0&1\\ 0&0&0&0&0 \end{bmatrix},\quad \mathbf{Q}^{10} = \begin{bmatrix} 0&0&0&0&0\\ 0&0&0&0&0\\ 1&0&0&0&0\\ 0&1&0&0&0\\ 0&0&1&0&0\\ 0&0&0&1&0\\ 0&0&0&0&0\\ 0&0&0&0&0\\ 0&0&0&0&0\\ 0&0&0&0&1 \end{bmatrix},$$

$$\mathbf{Q}^{11} = \begin{bmatrix} 0&0\\ 0&0\\ 0&0\\ 0&0\\ 1&0\\ 0&1\\ 0&0\\ 0&0\\ 0&0\\ 0&0 \end{bmatrix}.$$

Substituting interpolations (24), (25), (37), (38), (40) and (41) into the mixed variational Eq. (23) in conjunction with Eq. (20) and employing the analytical integration inside the element, one obtains the element equilibrium equations

$$\hat{\boldsymbol{\varepsilon}}^{r_1r_2} = \left(\mathbf{Q}^{r_1\,r_2}\right)^{\mathrm{T}}\mathbf{B}_u^{r_1r_2}\mathbf{U}, \tag{42}$$

$$\mathbf{H}^{r_1r_2} = \left(\mathbf{Q}^{r_1r_2}\right)^{\mathrm{T}}\mathbf{D}_{uu}\mathbf{Q}^{r_1r_2}\hat{\boldsymbol{\varepsilon}}^{r_1r_2} + \left(\mathbf{Q}^{r_1r_2}\right)^{\mathrm{T}}\mathbf{D}_{u\varphi}^{(\ell)}\mathbf{B}_{\varphi}^{(\ell)r_1r_2}\boldsymbol{\Phi}_{\ell},$$

$$\sum_{r_1,r_2}\frac{1}{3^{r_1+r_2}}\left(\mathbf{B}_u^{r_1r_2}\right)^{\mathrm{T}}\mathbf{Q}^{r_1r_2}\mathbf{H}^{r_1r_2} = \mathbf{F}_p,$$

$$\sum_{r_1,r_2}\frac{1}{3^{r_1+r_2}}\left(\mathbf{B}_{\varphi}^{(\ell)r_1r_2}\right)^{\mathrm{T}}\left[(\mathbf{D}_{u\varphi}^{(\ell)})^{\mathrm{T}}\mathbf{Q}^{r_1r_2}\hat{\boldsymbol{\varepsilon}}^{r_1r_2} - \mathbf{D}_{\varphi\varphi}^{(\ell)}\mathbf{B}_{\varphi}^{(\ell)r_1r_2}\boldsymbol{\Phi}_{\ell}\right] = \mathbf{F}_{\mathrm{q}}^{(\ell)},$$

where $\mathbf{F}_{\mathrm{p}}$ is the element-wise surface traction vector; $\mathbf{F}_{\mathrm{q}}^{(\ell)}$ is the element-wise electric force vector of the ℓth piezoelectric layer.

Eliminating further assumed strains and stress resultants from equilibrium Eqs. (42), we derive governing equations of the piezoelectric finite element

$$\begin{bmatrix} \mathbf{K}_{uu} & \mathbf{K}_{u\varphi}^{(\ell)} \\ \left(\mathbf{K}_{u\varphi}^{(\ell)}\right)^{\mathrm{T}} & \mathbf{K}_{\varphi\varphi}^{(\ell)} \end{bmatrix}\begin{bmatrix} \mathbf{U} \\ \boldsymbol{\Phi}_{\ell} \end{bmatrix} = \begin{bmatrix} \mathbf{F}_{\mathrm{p}} \\ \mathbf{F}_{\mathrm{q}}^{(\ell)} \end{bmatrix}, \tag{43}$$

where $\mathbf{K}_{uu}$ is the stiffness matrix; $\mathbf{K}_{u\varphi}^{(\ell)}$ is the piezoelectric stiffness matrix; $\mathbf{K}_{\varphi\varphi}^{(\ell)}$ is the dielectric stiffness matrix defined as

$$\mathbf{K}_{uu} = \sum_{r_1,r_2}\frac{1}{3^{r_1+r_2}}\left(\mathbf{B}_u^{r_1r_2}\right)^{\mathrm{T}}\mathbf{Q}^{r_1r_2}\left(\mathbf{Q}^{r_1r_2}\right)^{\mathrm{T}} \times \mathbf{D}_{uu}\mathbf{Q}^{r_1r_2}\left(\mathbf{Q}^{r_1r_2}\right)^{\mathrm{T}}\mathbf{B}_u^{r_1r_2}, \tag{44}$$

$$\mathbf{K}_{u\varphi}^{(\ell)} = \sum_{r_1,r_2}\frac{1}{3^{r_1+r_2}}\left(\mathbf{B}_u^{r_1r_2}\right)^{\mathrm{T}}\mathbf{Q}^{r_1r_2}\left(\mathbf{Q}^{r_1r_2}\right)^{\mathrm{T}}\mathbf{D}_{u\varphi}^{(\ell)}\mathbf{B}_{\varphi}^{(\ell)r_1r_2}, \tag{45}$$

$$\mathbf{K}_{\varphi\varphi}^{(\ell)} = -\sum_{r_1,r_2}\frac{1}{3^{r_1+r_2}}\left(\mathbf{B}_{\varphi}^{(\ell)r_1r_2}\right)^{\mathrm{T}}\mathbf{D}_{\varphi\varphi}^{(\ell)}\mathbf{B}_{\varphi}^{(\ell)r_1r_2}. \tag{46}$$

Remark 2. The element stiffness matrix $\mathbf{K}_{uu}$ possesses six zero eigenvalues as required for satisfaction of the general rigid-body motion representation. This is due to the fact that 22 assumed strain parameters are accepted according to approximation (40), whereas the EG solid-shell element has seven displacement degrees of freedom per node exactly.

Remark 3. It is worth noting that all matrices (44)–(46) require only direct substitutions, that is, no inversion is needed for the EG piezoelectric hybrid finite element formulation developed. This is unusual for the isoparametric hybrid/mixed shell element formulations.

Remark 4. The element matrices (44)–(46) are evaluated by using the analytical integration assuming additionally that a product $A_1A_2c_1^Mc_2^M$ in functional (20) does not vary inside the element and it is calculated at the element center. Therefore, the proposed EG piezoelectric solid-shell element formulation

is very economical and efficient compared to the conventional isoparametric piezoelectric finite element formulations because this improvement allows one to reduce the computational cost of numerical integration in the evaluation of the elemental matrices.

7. NUMERICAL EXAMPLES

The performance of the proposed EG piezoelectric four-node solid-shell element EG7P4 is evaluated with several problems extracted from the literature. The results are compared with those obtained by using the robust isoparametric degenerated and solid-shell elements, and the EG piezoelectric four-node solid-shell element EG6P4 based on the 6-parameter shell model [9].

7.1. Purely Mechanical Examples

Here, we consider two purely mechanical problems to verify the ability of the EG7P4 element to overcome shear, membrane, and thickness locking. A comparison with well-established isoparametric solid-shell elements based on the 6-parameter [21] and 7-parameter [22] models is presented.

7.1.1. Cantilever Curved Beam

It is well-known that isoparametric four-node shell elements are free from membrane locking. In this paper, the exact geometry four-node shell element is developed, which brings membrane locking back. To assess membrane locking and thickness locking as well, we consider a popular test, namely, a cantilever curved beam whose centerline is one quarter of the circle. The beam of the unit width is subjected to the shear tip load as shown in Figure 3.

Table 1 lists the results of solving a curved beam problem through using 10 four-node solid-shell elements [21, 22]. The transverse tip displacement is normalized with respect to the exact elasticity solution [23] of the plane stress problem, that is,

$$u_3(\pi/2) = -\frac{\pi F\left(R_1^2 + R_2^2\right)}{E\left[R_1^2 - R_2^2 + \left(R_1^2 + R_2^2\right)\ln R_2/R_1\right]},$$
$$R_1 = R - \frac{1}{2}h, \qquad R_2 = R + \frac{1}{2}h.$$

As can be seen, both EG piezoelectric solid-shell elements perform well even for large values of the slenderness ratio $S = R/h$.

TABLE 1
Normalized transverse displacement at the tip of the cantilever curved beam.

Slenderness ratio	$S = 10$	$S = 100$	$S = 500$	$S = 2000$
EG7P4	1.009	0.992	0.992	0.991
EG6P4	1.006	0.992	0.992	0.978
ANSγ-UL [22]*	1.00	0.99	0.96	–
ANS$\gamma\varepsilon$-HS [21]	1.001	0.997	0.997	–

*Results were measured from a graph by Sze et al. [21]

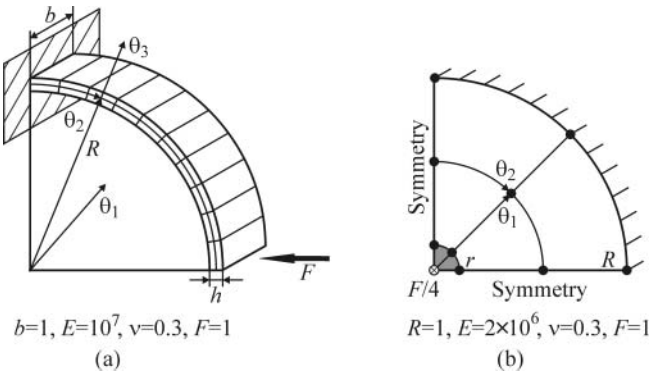

FIG. 3. Purely mechanical problems: (a) cantilever curved beam under the shear tip load and (b) clamped circular plate under the concentrated load.

7.1.2. Clamped Circular Plate under Concentrated Load

To investigate the capability of the proposed EG shell element to avoid shear locking, we study a clamped circular plate with a small rigid circular inclusion of the radius r at its center. Such a problem is also an excellent test to verify the analytical integration schemes developed. This is due to the facts that, first, we utilize just elemental nodes to evaluate the stiffness matrix, i.e., no Gauss sampling points are employed and, secondly, we deal with a shell of revolution with geometrical parameters

$$A_1 = 1, \quad A_2 = r + \theta_1, \quad k_1 = k_2 = 0, \quad \theta_1 \in [0,\ R - r]. \tag{47}$$

Owing to symmetry of the problem, only one quarter of the plate is discretized by regular meshes depicted in Figure 3. It has been established that the transverse central midplane displacement normalized with respect to the exact solution of the Kirchhoff plate theory practically does not depend on the radius of the rigid circular plate. The use of the 16×1 mesh of EG7P4 elements with $S = 1000$ yields the following results: $\bar{u}_3^{\mathrm{M}} = 0.9859$, 1.0014 and 1.0030 for $R/r = 10^2$, 10^4 and 10^6, respectively. Table 2 lists results of the convergence study for different $S = R/h$ and $R/r = 10^5$. It is seen that the EG7P4 element is free of shear locking.

7.2. Piezoelectric Actuator Examples

In this section, we consider four actuator benchmarks, which clearly show the convenience of referring to the EG shell element formulation to use coarse mesh configurations in deep curved actuators. The results are compared with those obtained utilizing the isoparametric hybrid strain nine-node solid-shell

TABLE 2
Convergence results through using the normalized transverse center point displacement $\bar{u}_3^{\mathrm{M}}$ of the clamped circular plate under a concentrated load for $R/r = 10^5$.

Mesh	2×1	4×1	8×1	16×1	2×2	4×2	8×2	16×2
$S = 100$	0.7724	0.9721	1.0016	1.0026	0.7730	0.9723	1.0016	1.0026
$S = 1000$	0.7801	0.9787	1.0013	1.0018	0.8196	0.9705	1.0006	1.0009
$S = 2000$	0.7897	0.9699	0.9964	0.9982	1.0562	1.0168	1.0286	1.0040

element ISP6P9 [4], ANS four-node degenerated-shell element Q_4TSF [24] and eight-node solid element C3D8E of Abaqus® employed in [24].

7.2.1. Simply Supported Plate with PZT Actuators

This example demonstrates the shape control of the laminated composite plate through bending actuation. A simply supported plate with PZT G1195 actuators bonded to the outer surfaces is initially subjected to uniform pressure of 200 Pa [25]. The plate core is composed of six graphite/epoxy layers with stacking sequence $[0/90/0]_{\mathrm{S}}$. The geometrical data of the problem are presented in Figure 4. The non-vanishing material parameters for graphite/epoxy are $E_{11} = 150$ GPa, $E_{22} = E_{33} = 9$ GPa, $\nu_{12} = \nu_{13} = 0.3$, $\nu_{23} = 0.49$, $G_{12} = G_{13} = 7.1$ GPa, $G_{23} = 3$ GPa; for PZT G1195 are $E = 63$ GPa, $\nu = 0.3$, $G = 24.2$ GPa, $d_{31} = d_{32} = 254$ pm/V. The piezoceramic layers are polarized in opposite directions parallel to the θ_3-direction and subjected to a constant voltage of $\hat{\varphi} = 15$ V and 27 V. The electrodes on the interfaces are assumed to be at the zero potential.

Due to symmetry of the problem, only one quarter of the plate is modeled by the uniform 8×8 mesh of EG7P4 elements. Figure 4 shows the distribution of the transverse midplane displacement along the θ_1- axis compared with numerical results [4, 9] derived by using identical node spacing. It is seen that all corresponding results are in a good agreement but the EG finite element code is less expensive because no matrix inversions are needed and it is based on the 3D analytical integration.

7.2.2. Cantilever Cylindrical Shell with PZT Actuators

Further, we investigate a response of the cantilever laminated cylindrical shell [25] made of above six graphite/epoxy layers with PZT G1195 actuators attached to the bottom and top surfaces and polarized in opposite directions parallel to the thickness direction. The geometrical and material properties of the shell are given in Figure 5 and Section 7.2.1. A ply orientation $[30/30/0]_{\mathrm{S}}$ has been employed to induce the twisting actuation. Both piezoelectric layers are grounded on the interfaces and loaded at the outer surfaces by the electric potential of $\hat{\varphi} = 100$ V.

Figure 5 displays the tip midsurface displacement $w_1 = 10^3 u_3^M(a, b/2)/b$ and the twist $w_2 = 10^3(u_3^M(a, b) - u_3^M(a, 0))/b$ versus a dimensionless radius of the curvature of its surface. The results have been derived with the 16×16 mesh of EG7P4 elements and are compared with finite element solutions [4, 9] through using identical node spacing. As can be seen, both EG solid-shell elements perform well again.

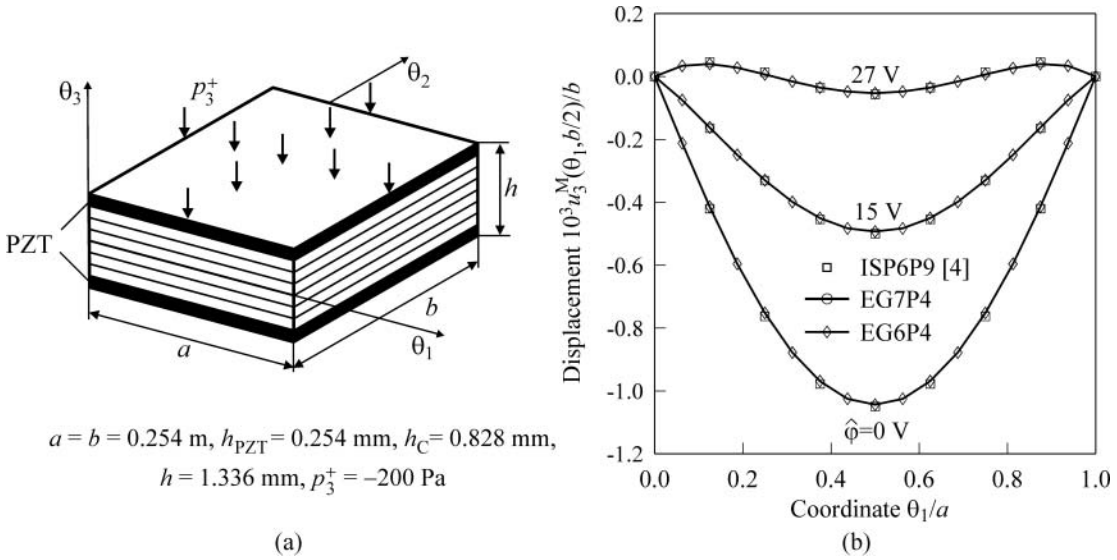

FIG. 4. Simply supported plate with PZT actuators: (a) geometry and (b) transverse midplane displacement.

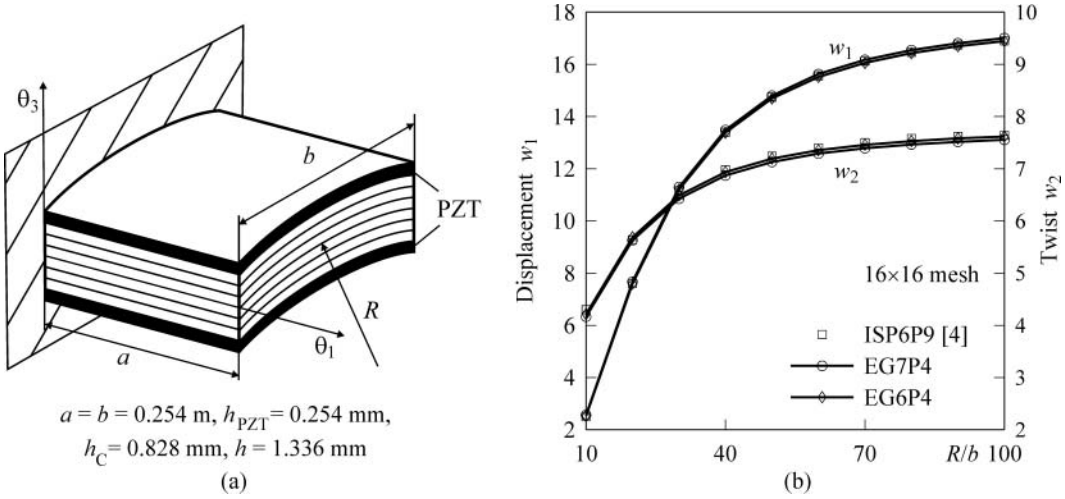

FIG. 5. Cantilever cylindrical shell with PZT actuators: (a) geometry and (b) tip midsurface displacement w_1 and twist w_2.

7.2.3. Cantilever Hyperbolic Shell with PVDF Actuators

To demonstrate the high coarse-mesh accuracy of the EG piezoelectric solid-shell element developed, we consider a six-layer graphite/epoxy hyperbolic shell covered with PVDF actuators on the bottom and top surfaces [9]. The material properties of PVDF are taken to be $E = 2$ GPa, $\nu = 0.29$ and $d_{31} = d_{32} = 23$ pm/V, whereas the material properties of graphite/ epoxy are presented in Section 7.2.1. The geometrical parameters of the shell can be written as follows:

$$A_1 = \sqrt{1 + \frac{\mu^2 z^2}{A_2^2}}, \qquad A_2 = r\sqrt{1 + \frac{\mu z^2}{r^2}},$$
$$z = \theta_1 \in [0,\ a], \tag{48}$$
$$k_1 = -\frac{\mu r^2}{A_1^3 A_2^3}, \qquad k_2 = \frac{1}{A_1 A_2}, \qquad \mu = \frac{R^2 - r^2}{a^2}.$$

The hyperbolic shell is assumed to be clamped on one of its edges as shown in Figure 6 and two stacking sequences $[0/90/0]_S$ and $[\gamma/\gamma/0]_S$ are studied, where γ is the angle between the asymptotic line and the tangent to the meridian. This angle is measured in the clockwise direction and may be evaluated by means of a simple formula [9, 19]

$$\cos\gamma = \frac{A_1}{\sqrt{1+\mu}}. \tag{49}$$

The electric potential at the outer surfaces of the piezoelectric layers is equal to the externally applied voltage of 1 V and at interfaces is treated as zero. Due to the opposite polarization of actuators, they will induce bending moments into the shell body and, therefore, in the case of the second ply sequence the twisting deformation will be generated.

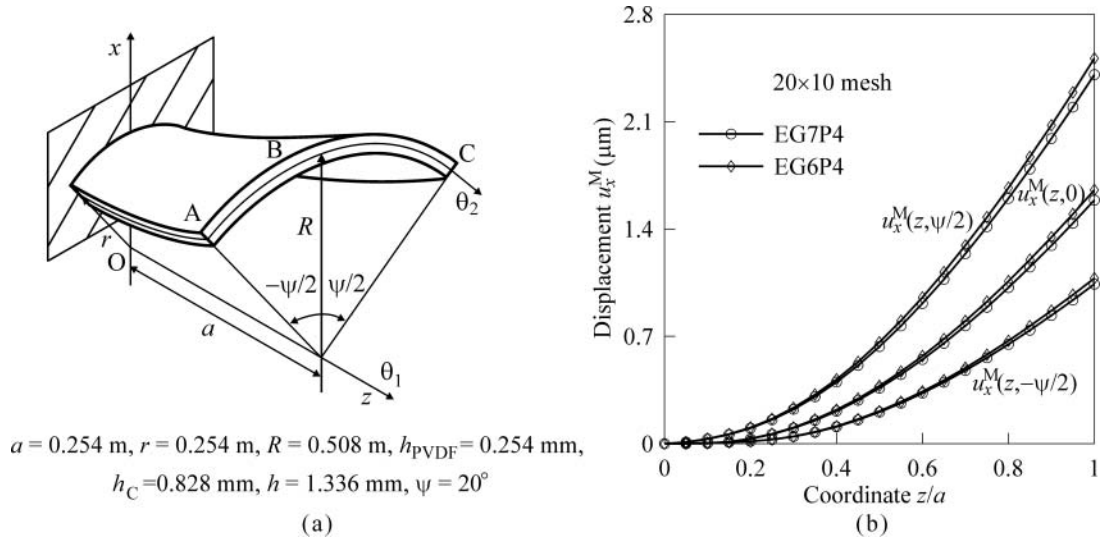

FIG. 6. Cantilever hyperbolic shell with PVDF actuators: (a) geometry and (b) midsurface displacements in the x-direction for the ply orientation $[\gamma/\gamma/0]_s$.

TABLE 3
Convergence results through using the tip midsurface displacement u_x^{M} (μm) of the cantilever hyperbolic shell (blanks in the u_x^{M}(B) row are explained utilizing too coarse mesh in which point B does not belong to a set of the element nodes).

	$[0/90/0]_{\mathrm{S}}$				$[\gamma/\gamma/0]_{\mathrm{S}}^{*}$			
Mesh	3×1	6×2	12×4	24×8	3×1	6×2	12×4	24×8
u_x^{M} (A)	0.4806	0.5798	0.5943	0.5954	1.009	0.930	1.018	1.041
u_x^{M} (B)		0.5231	0.5367	0.5377		1.462	1.560	1.589
u_x^{M} (C)	0.4806	0.5798	0.5943	0.5954	2.307	2.271	2.373	2.408

*The angle γ is calculated by means of Eqs. (48) and (49)

A shell is discretized with regular meshes of EG7P4 elements. Figure 6 shows the distribution of the midsurface displacement in the x-direction u_x^M along the z-axis and a comparison with results [9]. One can observe that the 6-parameter shell model overestimates the tip displacement values by 4.2%. Additionally, Table 3 lists results of the convergence study. It should be noted that these results could not be easily achieved by the conventional isoparametric piezoelectric solid-shell elements with such coarse mesh configuration.

7.2.4. Spiral Actuator

Consider a spiral actuator [24] made of the PZT-5H ceramic with the following properties: $c_{11} = c_{22} = 127.205\,\mathrm{GPa}$, $c_{12} = 80.212\,\mathrm{GPa}$, $c_{13} = c_{23} = 84.670\,\mathrm{GPa}$, $c_{33} = 117.436\,\mathrm{GPa}$, $c_{44} = c_{55} = 22.988\,\mathrm{GPa}$, $c_{66} = 23.474\,\mathrm{GPa}$, $e_{31} = e_{32} = -6.62\,\mathrm{C/m^2}$, $e_{33} = 23.24\,\mathrm{C/m^2}$, $e_{24} = e_{15} = 17.03\,\mathrm{C/m^2}$, $\in_{11}=\in_{22}= 15.05\,\mathrm{nF/m}$, $\in_{33}= 13.01\,\mathrm{nF/m}$. The spiral, shown in Figure 7, consists of four turns and has external radii $r_{\min} = 1.875\,\mathrm{mm}$ and $r_{\max} = 15.2\,\mathrm{mm}$, an effective length $L = 215\,\mathrm{mm}$, and a width $b = 3.75\,\mathrm{mm}$. The geometrical parameters of the spiral shell can be represented as

$$
\begin{aligned}
&A_1 = 1, \quad A_2 = \sqrt{a^2 + r^2}, \\
&k_1 = 0, \quad k_2 = \frac{1}{A_2^3}\left(2a^2 + r^2\right), \\
&r = r_{\min} + a\theta_2, \qquad \theta_2 \in [0,\ 8\pi\,],
\end{aligned}
\tag{50}
$$

where r is the polar radius; a is the parameter, which controls the distance between successive turnings. The actuator is polarized in the thickness direction and subjected to a constant voltage $\Delta V = 100\,\mathrm{V}$.

A spiral shell is modeled by uniform meshes of EG7P4 elements. Table 4 lists the results of the convergence study due to mesh refinement considering the tangential and transverse midsurface displacements at the tip and a comparison with finite element solutions [24]. The reference solution has been provided by the Abaqus® solid element C3D8E with a fine mesh, that is, two elements across the thickness and 20 elements across the width but the number of elements across the length is not documented. As can be seen, the EG7P4 element allows us to utilize coarse meshes because the 16×1 mesh yields already

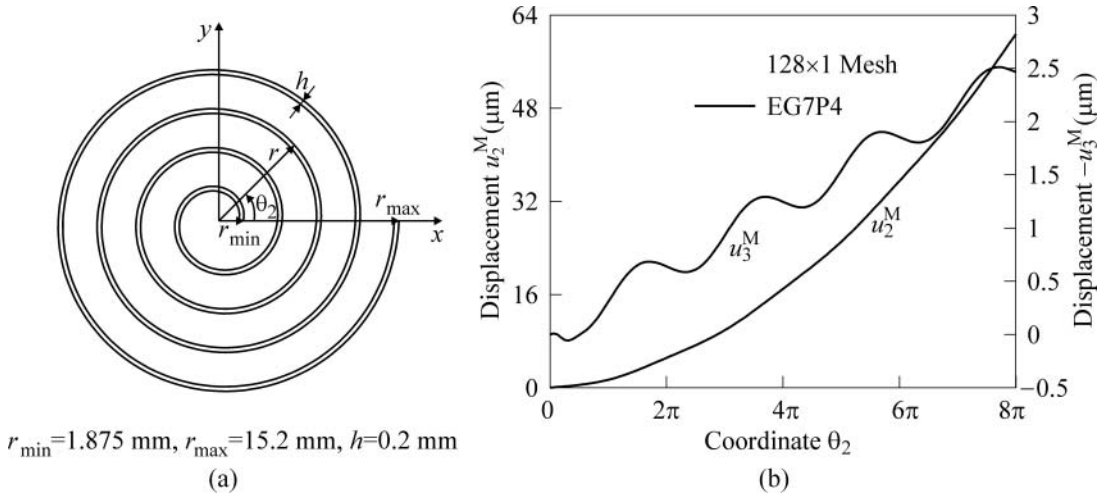

FIG. 7. Spiral actuator: (a) geometry and (b) midsurface displacements.

TABLE 4
Convergence results through using the tip midsurface displacements of the spiral actuator.

Element mesh	EG7P4								Q_4TSF	C3D8E
	16 × 1	16 × 2	16 × 4	32×1	32 × 2	32×4	64 × 1	128 × 1		
$-u_3^{\mathrm{M}}$ (μm)	2.109	2.102	2.100	2.625	2.620	2.619	2.503	2.460	2.00	2.59
u_2^{M} (μm)	58.18	58.16	58.15	59.95	59.88	59.87	60.55	60.72	−0.62	41.47

a good answer for the tangential displacement. Note also that the 7-parameter shell model overestimates the tangential tip displacement by 40%. This can be explained by the fact that the layer-wise description [26, 27] should be employed. A comparison with the Q_4TSF element shows additionally that the d_{33}-effect [24] is of great importance for the analysis of deep actuators. Finally, we represent in Figure 7 the distribution of tangential and transverse midsurface displacements in the θ_2-direction.

7.3. Piezoelectric Sensor Examples

Herein, we study two sensor benchmarks, which demonstrate convincingly that the use of the layer-wise electric potential field in conjunction with the ESL shell theory [28] permits to model efficiently laminated piezoelectric structures. The piece-wise linear approximation of the electric potential in the thickness direction is written as

$$\varphi = \sum_n \left(\bar{N}_n^- \varphi_{n-1} + \bar{N}_n^+ \varphi_n\right), \qquad (51)$$

$$\bar{N}_n^A = \begin{cases} N_n^A, & \theta_3 \in [z_{n-1},\ z_n] \\ 0, & \theta_3 \notin [z_{n-1},\ z_n] \end{cases},$$

where $\varphi_{n-1}(\theta_1,\ \theta_2)$ and $\varphi_n(\theta_1,\ \theta_2)$ are the electric potentials of the bottom and top surfaces of the nth layer; N_n^A are the Lagrange polynomials of the first order defined by Eq. (9). The layer-wise description (51) can be utilized to describe the higher order distribution of the electric potential through the thickness of the piezoelectric layer. This is achieved by the subdivision of the ℓth piezoelectric layer into I_ℓ fictitious discrete layers.

7.3.1. *Cantilever Bimorph Beam*

Let us consider a bimorph pointer consisting of two identical PVDF layers polarized in opposite directions parallel to the θ_3-direction. The material properties are assumed to be $E = 2$ GPa, $\nu = 0$, $e_{31} = e_{32} = 0.046\,\mathrm{C/m^2}$, $\in_{11}=\in_{22}=\in_{33}= 0.1062$ nF/m. A cantilever bimorph beam depicted in Figure 8 is subjected to the tip load $F = 0.025437N$, which produces a transverse tip displacement of 10 mm.

The distribution of the sensor voltage on the top surface in the length direction is displayed in Figure 8. A comparison with finite element solutions [8, 29, 30] is also presented. In the finite element model [30], there are five separate electrodes, which cover the full bimorph surface. Each electrode being an equipotential surface must have a constant voltage that reduces

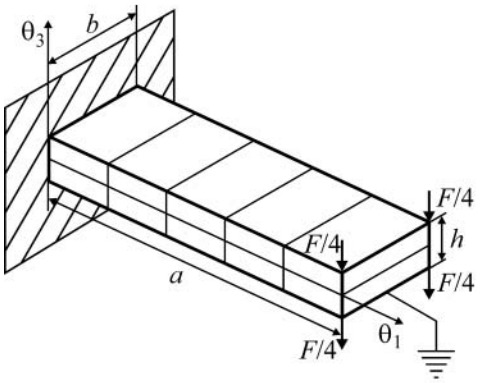

$a = 100$ mm, $b = 5$ mm, $h_{\mathrm{PVDF}} = 0.5$ mm, $h = 1$ mm,
$F = 0.025437\ N$

(a)

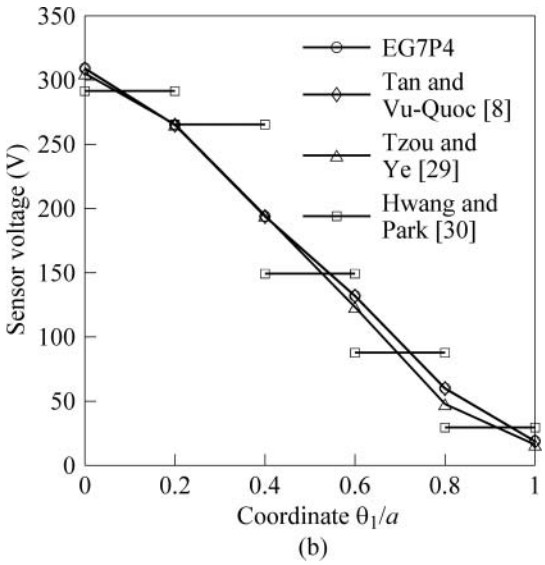

(b)

FIG. 8. Cantilever bimorph beam under the tip load: (a) geometry and (b) sensor voltage distribution.

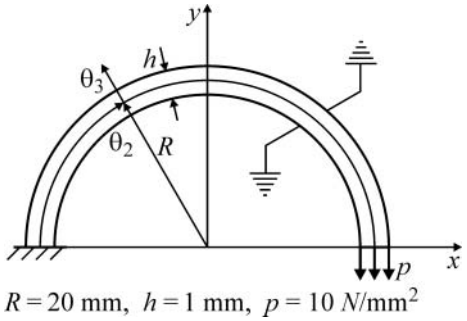

FIG. 9. Cantilever piezoelectric cylindrical shell under the tip load.

the number of electric variables to the number of electrodes. It is apparent that the equipotentiality condition of the electrodes leads to the step distribution shown in Figure 8. However, it is possible to have point electrodes [13] that would produce the sensor voltage distribution according to Tzou and Ye [29], Tan and Vu-Quok [8] and the present development.

7.3.2. Cantilever Piezoelectric Cylindrical Shell

Finally, we study the response of the cantilever piezoelectric cylindrical shell made of the PZT-5H ceramic. The geometrical parameters are chosen as follows: the radius of the midsurface $R = 20\,\text{mm}$, the width $b = 5\,\text{mm}$ and the thickness $h = 1\,\text{mm}$. The material properties of the shell are presented in Section 7.2.4. The shell is subjected to a distributed load $p = 10\,\text{N/mm}^2$ at its free end as shown in Figure 9. The piezoelectric ceramic is poled in the θ_3-direction and the electrodes on the bottom and top surfaces are grounded.

Table 5 lists the circumferential tip midsurface displacement derived using linear ($I_1 = 1$) and piece-wise linear ($I_1 = 2$) approximations of the electric potential through the shell thickness. A comparison with the ANS four-node degenerated-shell element Q_4TSF [24] and the 20-node piezoelectric solid element C3D20E of Abaqus® is also given. A reference solution was derived in [24] employing a fine mesh with four C3D20E elements across the thickness of the shell. It is seen that both finite element solutions of the purely mechanical problem corresponding to the linear electric potential variation agree closely. Note that the use of the piece-wise linear assumption for the electric potential underestimates the reference displacement by 1.5%. One can achieve better results if the quadratic electric potential approximation is employed.

TABLE 5
Circumferential tip midsurface displacement of the piezoelectric cylindrical shell.

Element	EG7P4 (64×1 mesh)		Q_4TSF [24]		C3D20E [24]
Potential	Linear	Piece-wise	Linear	Quadratic	Quadratic
$u_2^M(10^{-2}\text{m})$	7.469	6.479	7.523	6.555	6.581

8. CONCLUSIONS

A new piezoelectric laminated solid-shell model has been developed. This model is based on the objective strain-displacement relationships of the first-order 7-parameter ESL shell theory, which are invariant under all rigid-body shell motions. The simple and efficient hybrid stress-strain piezoelectric curved four-node solid-shell element is based on the original approach in which displacement vectors of outer and middle surfaces are introduced but resolved, in contrast with the isoparametric solid-shell element formulation, in the reference surface frame. It is remarkable that all elemental matrices require only direct substitutions and they are evaluated by using the 3D analytical integration. So, our EG piezoelectric solid-shell element is economical compared to conventional isoparametric finite elements because it additionally allows using very coarse meshes.

ACKNOWLEDGMENTS

This research was supported by the Russian Ministry of Education and Science under Grant No 2.1.1/660.

REFERENCES

1. A. Benjeddou, Advances in Piezoelectric Finite Element Modeling of Adaptive Structural Elements: A Survey, Comput. Struct., vol. 76, pp. 347–363, 2000.
2. K. Y. Sze, Three-Dimensional Continuum Finite Element Models for Plate/Shell Analysis, Prog. Struct. Eng. Mater., vol. 4, pp. 400–407, 2002.
3. K.Y. Sze, L.Q. Yao, and S. Yi, A Hybrid Stress ANS Solid-Shell Element and its Generalization for Smart Structure Modeling. Part II—Smart Structure Modeling, Int. J. Numer. Meth. Eng., vol. 48, pp. 565–582, 2000.
4. S. Lee, N.S. Goo, H.C. Park, K.J. Yoon, and C. Cho, A Nine-Node Assumed Strain Shell Element for Analysis of a Coupled Electro-Mechanical System, Smart Mater. Struct., vol. 12, pp. 355–362, 2003.
5. S. Zheng, X. Wang, and W. Chen, The Formulation of a Refined Hybrid Enhanced Assumed Strain Solid Shell Element and its Application to Model Smart Structures Containing Distributed Piezoelectric Sensors/Actuators, Smart Mater. Struct., vol. 13, pp. N43–N50, 2004.
6. S. Klinkel, and W. Wagner, A Geometrically Non-Linear Piezoelectric Solid Shell Element Based on a Mixed Multi-Field Variational Formulation, Int. J. Numer. Meth. Eng., vol. 65, pp. 349–382, 2006.
7. S. Klinkel, and W. Wagner, A Piezoelectric Solid Shell Element Based on a Mixed Variational Formulation for Geometrically Linear and Nonlinear Applications, Comput. Struct., vol. 86, pp. 38–46, 2008.
8. X.G. Tan, and L. Vu-Quoc, Optimal Solid Shell Element for Large Deformable Composite Structures with Piezoelectric Layers and Active Vibration Control, Int. J. Numer. Meth. Eng., vol. 64, pp. 1981–2013, 2005.
9. G.M. Kulikov, and S.V. Plotnikova, Geometrically Exact Four-Node Piezoelectric Solid-Shell Element, Mech. Advanced Mater. Struct., vol. 15, pp. 199–207, 2008.

10. S.V. Plotnikova, and M.G. Kulikov, Analysis of Composite Shells with Piezoelectric Patches, Trans. Tambov State Tech. Univ., vol. 15, pp. 380–391, 2009 (in Russian).
11. G.M. Kulikov, and S.V. Plotnikova, Simple and Effective Elements Based upon Timoshenko-Mindlin Shell Theory, Comput. Meth. Appl. Mech. Eng., vol. 191, pp. 1173–1187, 2002.
12. G.M. Kulikov, and S.V. Plotnikova, Equivalent Single-Layer and Layer-Wise Shell Theories and Rigid-Body Motions. Part I—Foundations, Part II—Computational Aspects, Mech. Advanced Mater. Struct., vol. 12, pp. 275–283; 331–340, 2005.
13. H.S. Tzou, Piezoelectric Shells: Distributed Sensing and Control of Continua, Kluwer-Academic, Dordrecht, 1993.
14. R.A. Arciniega, and J.N. Reddy, Tensor-Based Finite Element Formulation for Geometrically Nonlinear Analysis of Shell Structures, Comput. Meth. Appl. Mech. Eng., vol. 196, pp. 1048–1073, 2007.
15. G.M. Kulikov, and S.V. Plotnikova, Finite Rotation Geometrically Exact Four-Node Solid-Shell Element with Seven Displacement Degrees of Freedom, Comput. Model. Eng. Sci., vol. 28, pp. 15–38, 2008.
16. K.Y. Sze, X.-M. Yang, and H. Fan, Electric Assumption for Piezoelectric Laminate Analysis, Int. J. Solids Struct., vol. 41, pp. 2363–2382, 2004.
17. S.V. Gopinathan, V.V. Varadan, and V.K. Varadan, A Review and Critique of Theories for Piezoelectric Laminates, Smart Mater. Struct., vol. 9, pp. 24–48, 2000.
18. A. Benjeddou, J.-F. Deü, and S. Letombe, Free Vibrations of Simply-Supported Piezoelectric Adaptive Plates: an Exact Sandwich Formulation, Thin-Walled Struct., vol. 40, pp. 573–593, 2002.
19. G.M. Kulikov, and S.V. Plotnikova, Geometrically Exact Assumed Stress-Strain Multilayered Solid-Shell Elements Based on the 3D Analytical Integration, Comput. Struct., vol. 84, pp. 1275–1287, 2006.
20. G.M. Kulikov, Refined Global Approximation Theory of Multilayered Plates and Shells, J. Eng. Mech., vol. 127, pp. 119–125, 2001.
21. K.Y. Sze, and L.Q. Yao, A Hybrid Stress ANS Solid-Shell Element and its Generalization for Smart Structure Modelling. Part I—Solid-Shell Element Formulation, Int. J. Numer. Meth. Eng., vol. 48, pp. 545–564, 2000.
22. H. Parisch, A Continuum-Based Shell Theory for Non-Linear Applications, Int. J. Numer. Meth. Eng., vol. 38, pp. 1855–1883, 1995.
23. S.P. Timoshenko, and J.N. Goodier, Theory of Elasticity, 3rd edition, McGraw-Hill, New-York, 1970.
24. W. Zouari, T. Ben Zineb, and A. Benjeddou, A FSDT-MITC Piezoelectric Shell Finite Element with Ferroelectric Non-Linearity, J. Intel. Mater. Systems Struct., vol. 20, pp. 2055–2075, 2009.
25. H. Kioua, and S. Mirza, Piezoelectric Induced Bending and Twisting of Laminated Composite Shallow Shells, Smart Mater. Struct., vol. 9, pp. 476–484, 2000.
26. G.M. Kulikov, Strain-Displacement Relationships that Exactly Represent Large Rigid Displacements of a Shell, Mech. Solids, vol. 39, pp. 105–113, 2004.
27. G.M. Kulikov, and E. Carrera, Finite Deformation Higher-Order Shell Models and Rigid-Body Motions, Int. J. Solids Struct., vol. 45, pp. 3153–3172, 2008.
28. D.A. Saravanos, Mixed Laminate Theory and Finite Element for Smart Piezoelectric Composite Shell Structures, AIAA J., vol. 35, pp. 1327–1333, 1997.
29. H.S. Tzou, and R. Ye, Analysis of Piezoelastic Structures with Laminated Piezoelectric Triangle Shell Elements, AIAA J., vol. 34, pp. 110–115, 1996.
30. W.-S. Hwang, and H.C. Park, Finite Element Modeling of Piezoelectric Sensors and Actuators, AIAA J., vol. 31, pp. 930–937, 1993.

APPENDIX A

The mechanical, piezoelectric, and dielectric constitutive matrices introduced in Section 5 are given by

$$\mathbf{D}_{uu} = \begin{bmatrix} D_{11}^{00} & D_{11}^{01} & D_{12}^{00} & D_{12}^{01} & D_{13}^{00} & D_{13}^{01} & D_{16}^{00} & D_{16}^{01} & 0 & 0 \\ & D_{11}^{11} & D_{12}^{01} & D_{12}^{11} & D_{13}^{01} & D_{13}^{11} & D_{16}^{01} & D_{16}^{11} & 0 & 0 \\ & & D_{22}^{00} & D_{22}^{01} & D_{23}^{00} & D_{23}^{01} & D_{26}^{00} & D_{26}^{01} & 0 & 0 \\ & & & D_{22}^{11} & D_{23}^{01} & D_{23}^{11} & D_{26}^{01} & D_{26}^{11} & 0 & 0 \\ & & & & D_{33}^{00} & D_{33}^{01} & D_{36}^{00} & D_{36}^{01} & 0 & 0 \\ & & & & & D_{33}^{11} & D_{36}^{01} & D_{36}^{11} & 0 & 0 \\ & & & & & & D_{66}^{00} & D_{66}^{01} & 0 & 0 \\ & & & & & & & D_{66}^{11} & 0 & 0 \\ & & & & & & & & D_{55} & D_{45} \\ \text{sym.} & & & & & & & & & D_{44} \end{bmatrix},$$

$$\mathbf{D}_{u\varphi}^{(\ell)} = \begin{bmatrix} 0 & 0 & 0 & 0 & m_\ell^0 e_{31}^{(\ell)} \\ 0 & 0 & 0 & 0 & m_\ell^1 e_{31}^{(\ell)} \\ 0 & 0 & 0 & 0 & m_\ell^0 e_{32}^{(\ell)} \\ 0 & 0 & 0 & 0 & m_\ell^1 e_{32}^{(\ell)} \\ 0 & 0 & 0 & 0 & m_\ell^0 e_{33}^{(\ell)} \\ 0 & 0 & 0 & 0 & m_\ell^1 e_{33}^{(\ell)} \\ 0 & 0 & 0 & 0 & m_\ell^0 e_{36}^{(\ell)} \\ 0 & 0 & 0 & 0 & m_\ell^1 e_{36}^{(\ell)} \\ k_\ell^0 e_{15}^{(\ell)} & k_\ell^1 e_{15}^{(\ell)} & k_\ell^0 e_{25}^{(\ell)} & k_\ell^1 e_{25}^{(\ell)} & 0 \\ k_\ell^0 e_{14}^{(\ell)} & k_\ell^1 e_{14}^{(\ell)} & k_\ell^0 e_{24}^{(\ell)} & k_\ell^1 e_{24}^{(\ell)} & 0 \end{bmatrix},$$

$$\mathbf{D}_{\varphi\varphi}^{(\ell)} = \begin{bmatrix} k_\ell^{00} \in_{11}^{(\ell)} & k_\ell^{01} \in_{11}^{(\ell)} & k_\ell^{00} \in_{12}^{(\ell)} & k_\ell^{01} \in_{12}^{(\ell)} & 0 \\ & k_\ell^{11} \in_{11}^{(\ell)} & k_\ell^{01} \in_{12}^{(\ell)} & k_\ell^{11} \in_{12}^{(\ell)} & 0 \\ & & k_\ell^{00} \in_{22}^{(\ell)} & k_\ell^{01} \in_{22}^{(\ell)} & 0 \\ & & & k_\ell^{11} \in_{22}^{(\ell)} & 0 \\ \text{sym.} & & & & h_\ell \in_{33}^{(\ell)} \end{bmatrix},$$

where

$$D_{ab}^{pq} = \sum_n m_n^{pq} C_{ab}^{(n)}, \qquad D_{cd} = \sum_n h_n C_{cd}^{(n)},$$

$$m_n^{pq} = \int_{z_{n-1}}^{z_n} \left(N^-\right)^{2-p-q} \left(N^+\right)^{p+q} d\theta_3,$$

$$m_\ell^p = \int_{z_{\ell-1}}^{z_\ell} \left(N^-\right)^{1-p} \left(N^+\right)^{p} d\theta_3,$$

$$k_\ell^{pq} = \int_{z_{\ell-1}}^{z_\ell} \left(N_\ell^-\right)^{2-p-q} \left(N_\ell^+\right)^{p+q} d\theta_3,$$
$$k_\ell^{p} = \int_{z_{\ell-1}}^{z_\ell} \left(N_\ell^-\right)^{1-p} \left(N_\ell^+\right)^{p} d\theta_3,$$

where the indices take the following values: $a,\ b = 1,\ 2,\ 3,\ 6$ and $c,\ d = 4,\ 5$, and $p,\ q = 0,\ 1$.

APPENDIX B

The column matrices $\mathbf{\Lambda}^A_{i\alpha r}$ and $\mathbf{\Pi}^A_{ir}$ of order 28×1, and the column matrices $\mathbf{\Xi}^A_{\alpha r}$ and $\mathbf{\Xi}^{(\ell)}_{3r}$ of order 8×1 introduced in Section 6 are evaluated as

$$\left(\mathbf{\Lambda}^A_{\alpha\alpha r}\right)_{\omega^A+\alpha+7(s-1),1} = d_{\alpha rs}, \quad \left(\mathbf{\Lambda}^A_{\alpha\alpha r}\right)_{\omega^A+\beta+7(s-1),1} = \delta_{rs} B_{\beta s},$$
$$\left(\mathbf{\Lambda}^A_{\alpha\alpha r}\right)_{\omega^A+3+7(s-1),1} = \delta_{rs} k_{\alpha s}, \quad \left(\mathbf{\Lambda}^A_{\beta\alpha r}\right)_{\omega^A+\beta+7(s-1),1} = d_{\alpha rs},$$
$$\left(\mathbf{\Lambda}^A_{\beta\alpha r}\right)_{\omega^A+\alpha+7(s-1),1} = -\delta_{rs} B_{\beta s}, \quad \text{for } \beta \neq \alpha,$$
$$\left(\mathbf{\Lambda}^A_{3\alpha r}\right)_{\omega^A+3+7(s-1),1} = d_{\alpha rs}, \quad \left(\mathbf{\Lambda}^A_{3\alpha r}\right)_{\omega^A+\alpha+7(s-1),1} = -\delta_{rs} k_{\alpha s},$$
$$\left(\mathbf{\Pi}^A_{\alpha r}\right)_{\alpha+7(s-1),1} = -\delta_{rs}/h, \quad \left(\mathbf{\Pi}^A_{\alpha r}\right)_{3+\alpha+7(s-1),1} = \delta_{rs}/h,$$
$$\left(\mathbf{\Pi}^A_{3r}\right)_{3+7(s-1),1} = (-1)^{\mu^A} \delta_{rs} \left(2\mu^A - 3\right)/h,$$
$$\left(\mathbf{\Pi}^A_{3r}\right)_{6+7(s-1),1} = -(-1)^{\mu^A} \delta_{rs} \left(1 + 2\mu^A\right)/h,$$
$$\left(\mathbf{\Pi}^A_{3r}\right)_{7+7(s-1),1} = (-1)^{\mu^A} 4\delta_{rs}/h,$$
$$\left(\mathbf{\Xi}^A_{\alpha r}\right)_{\mu^A+1+2(s-1),1} = d_{\alpha rs}, \quad \left(\mathbf{\Xi}^{(\ell)}_{3r}\right)_{1+2(s-1),1} = -\delta_{rs}/h_\ell,$$
$$\left(\mathbf{\Xi}^{(\ell)}_{3r}\right)_{2+2(s-1),1} = \delta_{rs}/h_\ell,$$

where δ_{rs} is the Kronecker delta and

$$d_{\alpha rs} = \frac{1}{4\ell_\alpha A_{\alpha r}} n_{\alpha s} \left(1 + n_{\beta r} n_{\beta s}\right) \quad \text{for } \beta \neq \alpha,$$

$$\omega^A = \begin{cases} 0 & \text{for } A = - \\ 3 & \text{for } A = + \end{cases}, \qquad \mu^A = \begin{cases} 0 & \text{for } A = - \\ 1 & \text{for } A = + \end{cases}.$$

The components of these column matrices not written out explicitly are zero and, as we remember, the indices $r,\ s$ run from 1 to 4.